Circulation in the Canary Basin: A Model/Data Analysis

MICHAEL A. SPALL

National Center for Atmospheric Research, Boulder, Colorado

The Canary Basin region of an eddy-resolving, primitive equation model of the North Atlantic is studied in terms of its time mean fields, eddy variability, and role in three fundamental oceanic processes. The model calculation was carried out by Bryan and Holland as the first Community Modeling Effort of the World Ocean Circulation Experiment. Each of the major currents in the region is represented in the model fields. Several aspects of the large-scale climatological density field which was used for initialization were improved by the dynamical model while other aspects were degraded. The major deficiencies in the model are the representation of the Mediterranean salt tongue and low values of the eddy kinetic energy. The difference in the model salt tongue is believed to be at least partially due to an insufficient treatment of the Mediterranean outflow. Several numerical parameterizations which may be partially responsible for the low eddy kinetic energy are suggested as topics for future study. The role of this region in the ventilation of the thermocline, meridional flux of temperature, and formation of the Mediterranean salt tongue is studied. In general, the model results compare well with the available data and, in some instances, suggest mechanisms for previously observed flow characteristics and possibly important phenomena which have not yet been observed. Final recommendations are made to both the modeling and observational communities for future activities in this region.

1. INTRODUCTION

The Canary Basin is roughly defined as the area extending from 40°W to the eastern coast and 10°N to 40°N. This region of the North Atlantic, which contains the eastern portion of the subtropical gyre, has traditionally been thought to be governed primarily by Sverdrup dynamics. Although this is generally reflected in the climatological data base, recent observational programs have confirmed the existence of mesoscale jets, eddies, and lenses in the region. Currents represented in the mean fields include the Azores Current, the Portugal Current, and the North Equatorial Current. The Azores Current separates from the Gulf Stream near the Grand Banks and flows into the Canary Basin just south of the Azores Islands. The Portugal Current flows to the south along the coast of Portugal and the North Equatorial Current flows to the north between 40°W and the coast of Africa. All three of these currents turn to the west and exit the Canary Basin between 10°N and 30°N. This flow system, combined with the presence of mesoscale eddies and lenses of undiluted Mediterranean water, makes this an interesting region for study.

The Canary Basin is important to the general circulation of the North Atlantic for several reasons. The poleward transport of heat is fundamental to the coupled ocean-atmosphere system and it is believed that this region contributes a significant portion to the total southward heat transport in the North Atlantic Basin [*Stramma and Isemer*, 1986]. This region is also central to the formation and maintenance of the Mediterranean salt tongue in the North Atlantic. Thirdly, the eastern region of the North Atlantic is believed to be important for the ventilation of the thermocline [*Luyten et al.*, 1983]. Knowledge of this interaction between the ocean and the atmosphere is important for coupled ocean-atmosphere, climate, and biological studies.

There have been many recent observational programs in the Canary Basin. Some of these efforts have been designed to study the general physical oceanography of the region while others have been aimed at specific processes or currents. A general survey of the large-scale (1000 km) property distributions in the eastern subtropical gyre is given by *Armi and Stommel* [1983]. *Gould* [1985] discusses the structure of the Azores Current through a combined analysis of hydrographic data, float data and sea surface temperature. A summary of what is known about the deep velocity fields based on current meter data is given by *Dickson et al.* [1985]. A series of studies from the "Kiel Warmwatersphere of the Atlantic" project (SFB133) has looked at the current distribution and seasonal variations [*Stramma*, 1984; *Stramma and Siedler*, 1988] and the role of the Canary Basin in the poleward flux of temperature [*Stramma and Isemer*, 1986; *Stramma and Isemer*, 1988]. Float programs by the Woods Hole Eastern Basin Study [*Price et al.*, 1986; *Zemanovic et al.*, 1988), W. J. Gould (private communication, 1989), and *Maillard and Käse* [1989] have been designed to investigate the general circulation and variability of the region. Hydrographic surveys by *Käse et al.* [1986], *Zenk et al.* [1989], and *Käse et al.* [1985] have helped to describe the water mass distribution, temperature variability, and geostrophic transports. The moored arrays of *Schmitz et al.* [1988] and *Zenk and Müller* [1988] have given direct measurements of the velocity and temperature fields and an estimate of the eddy variability in the region.

Previous numerical modeling studies in the Canary Basin have been limited to idealized thin jet representations of a single component of the basin current structure [*Kielmann and Käse*, 1987; *Käse et al.*, 1989]. These studies have been useful for the identification of possible processes active in the current under study but they do not relate those currents to the general circulation or observed statistical properties of the region. There are several reasons for the lack of extensive modeling studies in the Canary Basin. Because the primary forcing mechanisms of the Azores Current are not well known, fundamental process studies on its formation and maintenance and its relation to the general circulation

have been difficult. Eddy-resolving basin-scale calculations with realistic geometry, which may form the proper current structure, have previously not been available due to the computational expense. Limited region models are more affordable but the problem of providing the proper boundary conditions and coupling with the rest of the basin is a difficult one.

An eddy-resolving, primitive equation calculation of the North Atlantic has been carried out by *Bryan and Holland* [1989] at the National Center for Atmospheric Research. This calculation is the first experiment in the World Ocean Circulation Experiment (WOCE) Community Modeling Effort. The model provides a significant increase in resolution and physics compared with previous calculations with realistic geometry such that the fundamental processes responsible for water mass formation and hydrodynamic instabilities are both represented. In addition, representations of physical processes such as an upper mixed layer and the Mediterranean outflow are included. It is intended that the results of this model can be used to address questions on the role of the mesoscale in the general circulation of the North Atlantic as well as provide a new benchmark for the development of basin-scale numerical models. The analysis in this paper will concentrate on the Canary Basin region of the model fields.

A model/data comparison in the Canary Basin is potentially very useful. At present, enough data exist to indicate that the region is especially interesting and worthy of detailed study. The current data base may be used to identify some of the shortcomings of the model calculation and, as a result, provide considerations for the future design of similar numerical calculations and prompt more basic process-oriented modeling studies. Based on the model/data comparisons, the model fields may be used to extend estimates of relevant processes beyond that which is presently obtainable directly from the observations. In addition, the model may provide possible interpretations for observed flow characteristics. There are several observational programs in the area which are currently under way or being planned for basic study in the region; these include studies of the Mediterranean salt tongue and Meddy formation, mesoscale variability, and ventilation of the thermocline. It is hoped that the results of the model analysis presented in this paper may suggest interesting phenomena in the region and influence the development of these future observational programs.

A conclusive model/data comparison is difficult because of the complete four-dimensional nature of the model fields and the fact that the observations are taken from many disconnected programs which vary in spatial and temporal coverage and experimental objectives. Because the purpose of this paper is both to evaluate the model fields and to learn about the physical oceanography of the region, the analysis also follows a somewhat disconnected path. One of the problems with this type of investigation is that there are many criteria by which to evaluate and study the fields. The analysis presented in this paper falls into two categories: a direct comparison of dynamic variables and an indirect comparison via the study of the meridional flux of temperature, the ventilation of the thermocline, and the formation of the Mediterranean salt tongue. These quantities have been chosen because of the availability of observations for comparison, the importance to the general circulation of the North Atlantic, the potential for additional information not

available from observations, and relevance for future observational programs.

This paper is outlined as follows. In section 2, the dynamical model and physical assumptions are presented. Section 3 describes the basic velocity and density structure of the mean model fields and makes comparisons with available data. The eddy kinetic energy and role of the variability in instability processes is investigated in section 4. In section 5, the role of the Canary Basin region in three fundamental oceanic processes are investigated. Conclusions and recommendations are presented in section 6.

2. NUMERICAL MODEL

The numerical integration which is analyzed in this paper was carried out by *Bryan and Holland* [1989] at NCAR as the first experiment in the WOCE Community Modeling Effort. The model domain extends from 15°S to 65°N and from the west coast to the east coast of the Atlantic Basin. The horizontal discretization is $\frac{2}{5}°$ in longitude and $\frac{1}{3}°$ in latitude, giving approximately equal grid spacing of 35 km at 40°N. The vertical discretization uses 30 levels distributed over a maximum depth of 5500 m. The vertical spacing is nonuniform with a minimum of 35 m at the surface and expanding to 250 m at depths below 1000 m. Topography which was represented by a single grid point in the model was removed. The Mediterranean Basin is not included in this calculation; the treatment of the Mediterranean outflow will be discussed later in this section.

The numerical model used for the simulation is the three-dimensional primitive equation model developed by *Bryan and Cox* [1967]. The model was initialized at rest using the temperature and salinity fields of *Levitus* [1982] and integrated for 25 years. The form of the model equations and parameterizations developed for this experiment are summarized in Appendix A. As mentioned in the introduction, the main focus of this paper is the Canary Basin. Details of the experiment design and implementation, as well as a discussion of the basin-scale circulation, can be found in the work by *Bryan and Holland* [1989].

In the real ocean there is flow across the latitudes of the northern and southern boundaries of the model. This model does not attempt to treat the open boundary condition problem but imposes no flow through the northern and southern boundaries. The interaction with the rest of the world oceans is parameterized through a Newtonian damping of the model temperature and salinity fields back toward the monthly mean data set of Levitus. This restoration is done over a band of five grid points adjacent to the boundaries. The artificial reflection and generation of waves at the boundaries will be suppressed while it is hoped that some of the effects of interbasin exchange of water masses will still be included.

A similar Newtonian damping term is added to the tracer equations in the vicinity of the Mediterranean outflow and the Labrador Sea. There is no explicit flow through the Strait of Gibraltar but the net flux of temperature and salinity from this region is parameterized through this nonconservative term. Water parcels leaving the damping region will take on water properties characteristic of the climatological temperature and salinity field in this region. The damping in the Labrador Sea is required to maintain realistic sea temperatures over the shelf region where there is

extreme cooling to the atmosphere. Sea ice forms in the actual ocean but those processes are not included in the dynamical model.

The surface wind forcing is taken from the monthly mean winds derived by *Hellerman and Rosenstein* [1983]. The surface flux of temperature is derived from a relation for the surface heat flux based on the analysis of *Han* [1984]. The time scale of the surface heat flux depends on the latitude, longitude, time of year, and sea surface temperature but is on the order of 50 days. Because the surface flux of salt (or evaporation minus precipitation) is not well known, it is parameterized through a relaxation of the surface salinity toward the monthly mean climatology. It appears similar in form to the surface heat flux and uses a constant damping time of 50 days.

The mixed layer formulation is similar to the bulk kinetic energy model of *Camp and Elsberry* [1978]. The energy available for deepening of the mixed layer from wind work is converted into potential energy and distributed over the depth of the mixed layer. This model allows for a mixed layer which is of arbitrary depth down to a maximum of 800 m. Detrainment of the mixed layer is also included such that if the mixed layer depth shallows, the deeper remnants of the old mixed layer remain.

3. GENERAL DESCRIPTION

In this section, the basic characteristics of the model velocity and density fields in the Canary Basin will be discussed and compared with observed fields. Similarities, differences, and information not available from observations will be highlighted. Unless otherwise stated, the model fields are the mean fields averaged over the last two years of integration. The quantities to be analyzed are upper thermocline transport stream function, presence of Mediterranean water, deep velocity field, large-scale temperature and salinity structure, and water mass distribution.

3.1. Upper Thermocline Transports

The transport stream function for the upper 800 m of the model fields is shown in Figure 1a. For comparison purposes, the stream function calculated from historic hydro-

graphic data and Conductivity-temperature-depth (CTD) surveys is shown in Figure 1b , from *Stramma* [1984], (hereinafter referred to as S84). Note that Figure 1a. is plotted in degrees while Figure 1b is plotted in kilometers such that there is approximately 25% stretching in the longitude of Figure 1a. The overall description of the flow field in the upper thermocline is that of three distinct currents entering the region and all flowing toward the west between 10°N and 30°N. The Azores Current (AC) enters from the west near 32°N, turns to the south, and flows out to the west near 26°N. The Portugal Current (PC) flows to the south between the Azores Islands and the coast of Portugal, turns westward off the northwest coast of Africa and flows out of the region just south of the AC recirculation. The North Equatorial Current (NEC) enters from the south between the coast and 40°W, flows northward, and then turns to the west. A more detailed description of each of these currents follows.

The model produces an AC of 6–7 Sv entering the region near 32°N. The historical data base shows a somewhat stronger flow, 11 Sv, entering the region a little further to the north, near 35°N. The model current is narrower but this is probably due to the larger temporal and spatial smoothing in the historical data set compared to the model. Other measurements put the transport of the AC at 10 Sv in the upper 1500 m [*Gould*, 1985] and 2000 m [*Stramma and Isemer*, 1988]. The transport of the model fields over the upper 1500 m shows a very similar pattern to that in Figure 1a but with an AC transport of 9 Sv, in better agreement with the deeper estimates. The westward recirculation is very tight in the model. The AC enters the region south of 35°N and exits the region north of 25°N, spanning only 10° of latitude, whereas the recirculation in the climatology covers over 16°. Again, some of this smoothing may be due to the low-frequency variability of the subtropical gyre which is not represented in the 2-year mean model fields. There is only a weak indication in the model of the three-band structure seen in Figure 1b.

The PC is a broad, weak flow entering the region between the Azores Islands and Portugal with a total transport of 8 Sv. Transports estimated from observations along this section vary widely. The transport in Figure 1b is only about
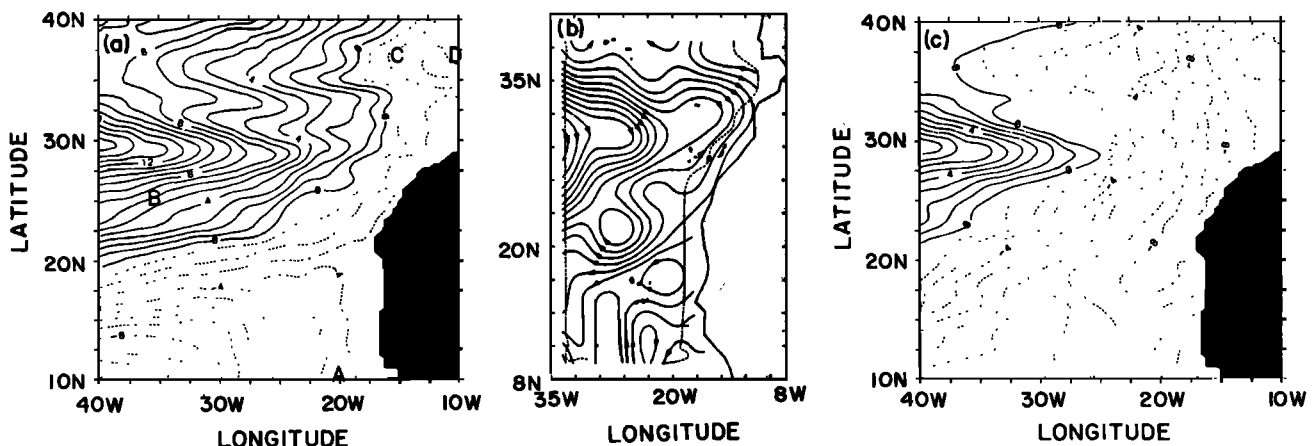
Fig. 1. Transport stream function, 0–800 m (contour interval 1 sv): (a) primitive equation velocity (letters A–D indicate the locations of T-S profiles shown in Figure 5), (b) historical data base, and (c) geostrophic balance.

3 Sv, while *Saunders* [1982] calculated a transport of 3–4 Sv in the upper 850 m. These are considerably less than that seen here, but some calculations based on observations place the transport much higher. *Sverdrup* [1942] estimated the total southward transport at 18 Sv while *Dietrich et al.* [1980] report a southward transport of 14 Sv between 0 and 1000 m from the International Geophysical Year data. There is a large-scale wave pattern superimposed on the southward flow of the PC in the model which is not observed in the climatological data base. The presence of these large-scale meanders is due to low-frequency waves which have remained in the 2 year average. A similar low-frequency zonal variability has been observed east of the Azores Islands in the float data of *Zemanovic et al.* [1988].

The NEC enters at 10°N between 40°W and the coast of Africa. The model transports 7 Sv in the upper 800 m. After entering the region, the water meets with the westward recirculation of the Azores Current and the Portugal Current and exits to the west. Figure 1b shows a weak indication of a NEC but there is not a coherent circulation. A seasonal analysis by *Stramma and Isemer* [1988] indicates a northward transport of between 0 and 7 Sv in the upper 1500 m. *Hellerman* [1980] used wind stress data to calculate the Sverdrup transports between 3 and 10 Sv at 23°W and 9 and 23 Sv at 38°W. The model transport compares well with these other estimates, being in the low range of the calculations based on the wind stress and at the high end of those based on the historical data base.

The geostrophic transport calculated from the model temperature and salinity fields is shown in Figure 1c. Rather than use a level of no motion, the geostrophic velocity was calculated relative to the primitive equation velocity at 1500 m. In this way, the differences are due only to ageostrophic effects in the upper 1500 m and not dependent on assumptions about a level of no motion. The geostrophic transport is similar to the full primitive equation transport in the region of the Azores and Portugal currents. The most striking difference between the two fields is in the NEC region. Where the full primitive equation fields show a slow but clear flow entering from the south and turning west, the geostrophic balance indicates only a weak flow entering from the south and flowing into the coast. The implication that the NEC transport is mostly ageostrophic is consistent with the conclusions of *Maillard and Käse* [1989] based on surface drifter data. The lack of a strong NEC in the analysis of S84 may be because the primary transport in the NEC is due to the Ekman flux. This also suggests that hydrographic surveys would not be a very good method to measure the total NEC transport.

3.2. Mediterranean Water, 1125 m

One of the most prominent features of the North Atlantic thermohaline field is the presence of the Mediterranean salt tongue. Shown in Figure 2a. is the salinity at 1125 m from the climatological data base of *Levitus* [1982]. This is a warm, salty water mass which is strongest between 1000 and 1200 m and extends westward from the Mediterranean outflow. The mechanisms of its formation and maintenance are not well known but are believed to be a mixed advection/diffusion process with isolated lenses of undiluted Mediterranean water (Meddies) acting as moving point sources [*Armi and Haidvogel*, 1982; *Richardson and*
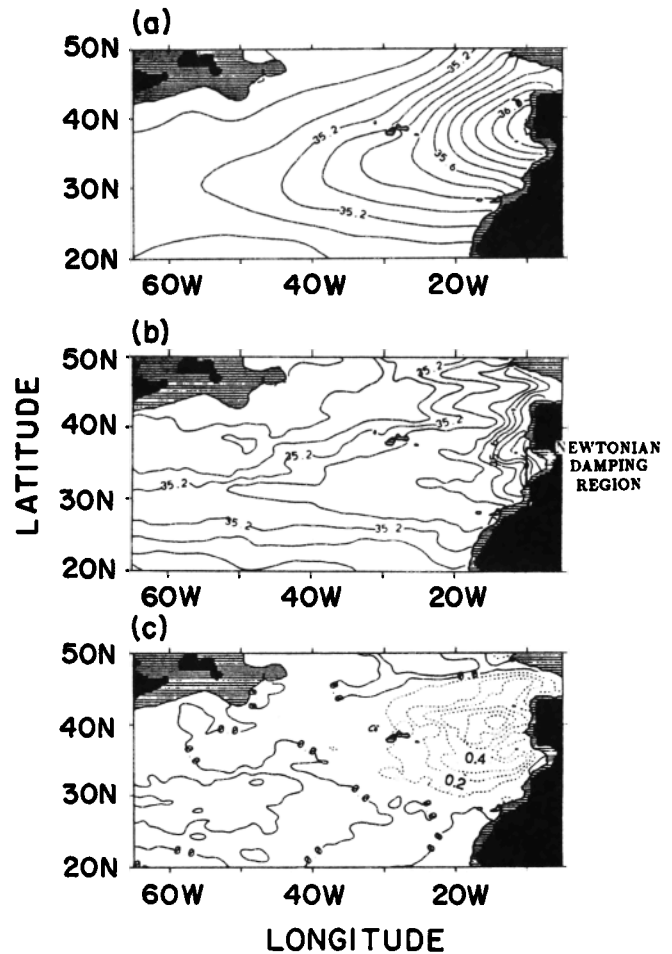
Fig. 2. Salinity at 1125 m (contour interval 0.1 ppt): (a) Levitus data, (b) mean model salinity years 24–25, and (c) difference between Levitus and model data.

Mooney, 1975]. In this section, the salinity field at 1125 m in the model will be compared with the Levitus salinity which was used to initialize the model. A more detailed discussion of the mechanisms of the salt tongue formation in the numerical model will be given in section 5.3.

The salinity at 1125 m averaged over the last 2 years of model integration is shown in Figure 2b. The salt tongue can be seen extending westward between 25°N and 35°N. There is a rapid decrease in salinity away from the eastern boundary, reduced from 36.0 ppt at the coast to approximately 35.4 ppt at 20°W. This is much less than the 35.6 ppt seen in Figure 2a at 20°W. The model salt tongue also has a highly variable structure in the meridional direction near the coast. There are two long filaments of higher-salinity water extending into the interior of the tongue past 20°W. Further to the west, the salt tongue is smoother and has a salinity almost 0.2 ppt greater than climatology. The model tongue has nearly constant salinity over most of the interior with sharp fronts marking its northern and southern extent. By contrast, the climatological tongue has nearly uniform gradients throughout its extent in the interior, possibly due to the extensive smoothing in the mapping procedure of Levitus. Due to its large spatial extent, synoptic representations of the entire salt tongue are not presently available.

As was mentioned in section 2, the model was initialized with temperature and salinity fields taken from Levitus. The difference in salinity between the last 2 years of the model calculation and the climatology which was used for initialization is shown in Figure 2c. In the vicinity of the damping region the difference is nearly zero; however, the low model salinity over most of the east and high model salinity in the west are clearly seen. Most of this restructuring of the salt tongue occurs over the first 20 years of model integration, this difference field remains nearly constant over the last 5 years. This indicates that the model is approaching a steady state which is significantly different from climatology.

3.3. Deep Velocity Field

A map of the average model velocity field at 2875 m is shown in Figure 3; fields averaged over the last 5 years of integration are qualitatively the same. The general sense of the flow field at this depth is that of two weakly connected anticyclonic circulations. The larger one is over the Canary Abyssal Plain and extends from 15°N to 30°N. A smaller circulation pattern also exists over the Madeira Abyssal Plain between 30°N and 37°N. The maximum time-averaged velocities in both circulations are on the order of 1 cm/s with most velocities much smaller. There is some flow from the Madeira Abyssal Plain over the Azores-Portugal Ridge (at 38°N) and into the Iberia Abyssal Plain. This transport is barotropic down to the top of the ridge, so that the total transport into the Iberia Abyssal Plain is estimated to be 0.25 to 0.5 Sv.

There have been some deep current meter and float measurements taken in this region but the data are sparse. Current meter measurements near 3000 m from several programs are found to have mean horizontal velocities on the order of 0.1 cm s^{-1} to 1.0 cm s^{-1} Dickson et al. [1985]. Although speculative, this data coverage in the Madeira Abyssal Plain indicates that the general circulation pattern is that of northward flow along 25°W with a weak southward flow in the east. There are also several current meters along the Azores-Portugal Ridge which indicate that there is

flow from the Madeira Abyssal Plain into the Iberia Abyssal Plain. The magnitudes of these mean currents are 1–2 cm s–1 but the coverage is inadequate for any meaningful estimate of the transport. The float data of Gould [1989] show a similar pattern near 3000 m with anticyclonic circulation in the region of 20°W to 26°W and 32°N to 36°N. These data are in general agreement with the magnitude and sense of the deep circulation found over the Madeira Abyssal Plain in the model calculation. No estimate of the deep flow pattern over the Canary Abyssal Plain can be made from present observations.

3.4. Meridional Sections

In this section, meridional sections of the model temperature and salinity fields are used to get a picture of the large-scale water mass distributions in the region. Observational programs in the Canary Basin have indicated that this is a region of complex water mass distributions with North Atlantic Central Water (NACW), South Atlantic Central Water (SACW), Antarctic Intermediate Water (AAIW), Mediterranean Water (MW), and North Atlantic Deep Water (NADW) all present. Although the model was initialized with a coarse representation of these water mass distributions, it is of interest to see to what extent the model maintains and refines the observed characteristics of the water properties.

Shown in Figure 4a. is the meridional section of the model temperature field along 20°W. In the upper ocean (≤ 600 m) there is a strong front located at 21°N. This boundary between the cooler SACW to the south and the warmer NACW to the north has been observed in CTD sections and was called the Central Water Boundary (CWB) by Zenk et al. [1989]. Another prominent feature of the upper thermocline is the presence of a layer of nearly isothermal water near 17°C between 27°N and 34°N, similar layers of water have been found in this region by several hydrographic surveys [Siedler et al., 1987; Gould 1985]. Siedler et al. [1987] hypothesize that this water is formed locally, near the Madeira Islands, and have called it Madeira Mode Water. The spreading of the 11°C to 12°C isotherms at the northern end of the section is similar to the spreading due to Mediterranean water seen in the sections of Käse et al. [1986] but it occurs at a shallower depth in the model.

The deeper temperature structure shows a gradual deepening of the isotherms from the south to the north between 10°N and 30°N. This is a signature of the bowl shape of the thermocline in the subtropical gyre. The warmer MW is deepening the isotherms between 22°N and 36°N. The eddy-like feature seen in the MW near 33°N is the interleaving of more pure MW with NACW of the interior seen in Figure 2b. The deep isotherms are nearly horizontal and less than 3°C, indicative of NADW. It should be noted that the model integration has not been carried out long enough for equilibration of the deep model fields.

Shown in Figure 4b is the meridional section of the model salinity along the longitude 20°W. Many of the features observed in the temperature section are apparent in the salinity section as well. The separation of the fresh SACW from the saltier NACW by the CWB is visible at 21°N. There is also evidence of the poleward transport of fresh water near the surface in this region by the Ekman transport. The Madeira Mode water is visible as a halostad near 36.3 ppt between
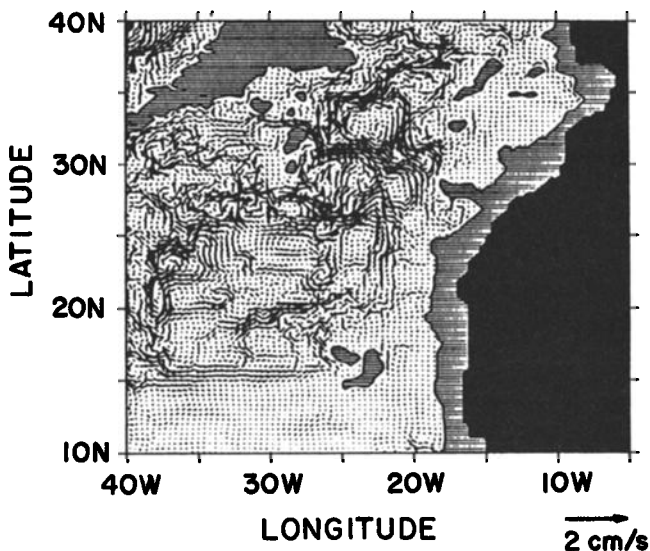
Fig. 3. Mean velocity field at 2875 m.

LATITUDE

40N
30N
20N
ION

40W 30W 20W IOW

LONGITUDE

2 cm/s

(a) TEMPERATURE (°C)

(b) SALINITY (ppt)

(c) TEMPERATURE (°C)

(d) SALINITY (ppt)
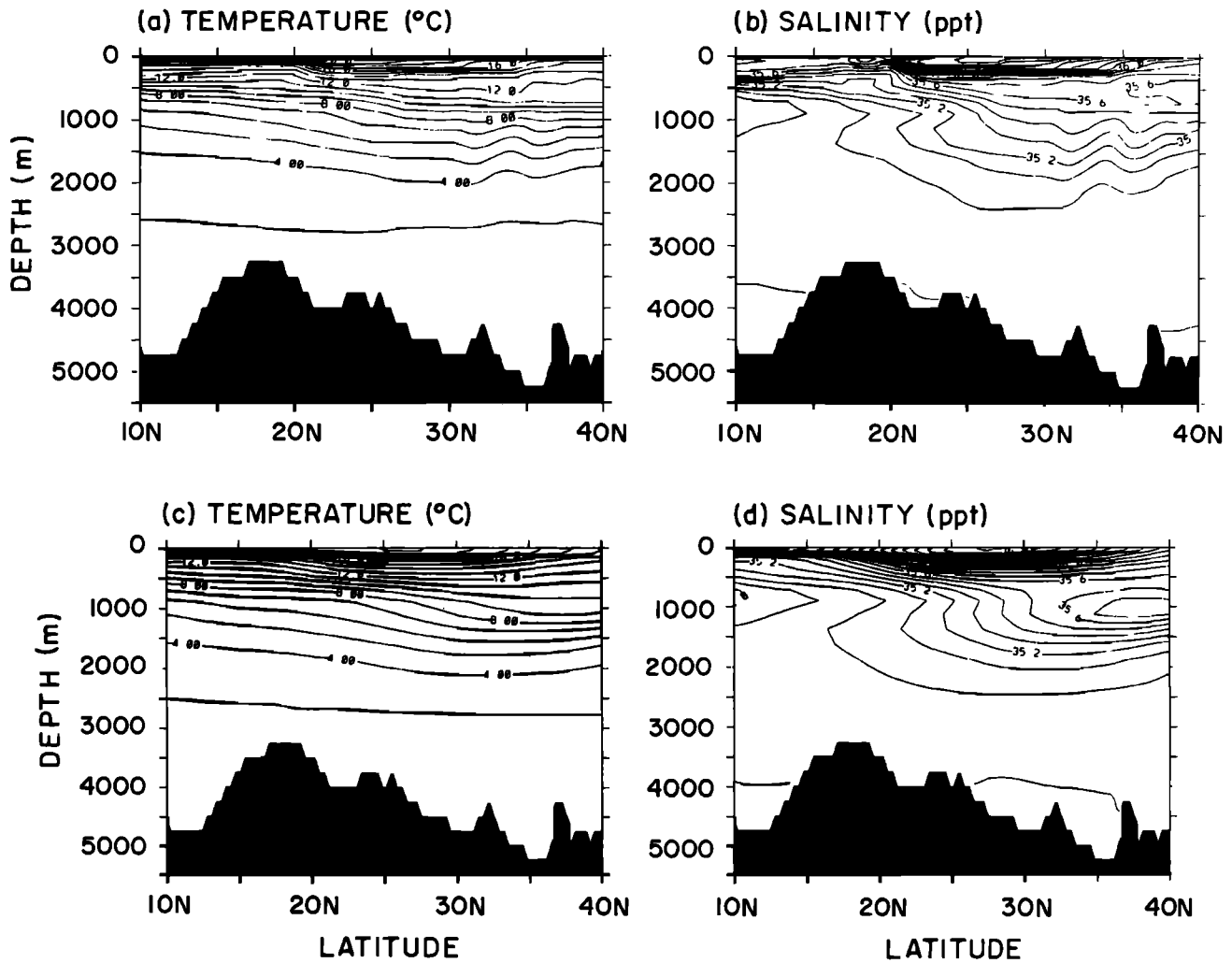
Fig. 4. Meridional section at 20°W: (a) model temperature (b) model salinity (c) Levitus temperature and (d) Levitus salinity.

28°N and 34°N. The separation of AAIW and MW at mid-depths is shown more clearly in the salinity field than it was in the temperature field. The fresher AAIW can be seen extending northward at 900 m overlying the MW extending to the south between 1200 m and 1400 m. A similar profile was found in a CTD section taken in the area by *Zenk et al.* [1989]. To the north, a weak increase in salinity is found due to the core of the Mediterranean salt tongue. The interleaving of the MW with the NACW is seen in the salinity section as well. The deep salinity fields are nearly constant at near 34.9 ppt.

The extent to which the model has modified the climatology used for initialization can be seen by comparing the temperature and salinity sections in Figures 4a. and 4b with the same sections taken through the Levitus data in Figures 4c and d. In general, the Levitus data have the same tendencies as were discussed for the model sections but the features are much smoother due to the analysis procedure of Levitus. The model has modified the fields in several ways, some are in better agreement with small-scale structure observed in the region and others are in disagreement with what is known about the water mass distribution. The broadening of the 9° to 11°C isotherms and the 35.5 to 35.6 ppt salinity

contours associated with the intrusion of the Mediterranean salt tongue in the Levitus sections is significantly reduced by the model. This is consistent with the weak representation of the salt tongue in the model at 1125 m discussed in section 3.2. The model has also reduced the strength of the AAIW extending into the region from the south at 900 m. Because the source of AAIW is south of the southern model boundary, its reduction may be a result of the Newtonian damping used to approximate the interbasin exchanges at the boundary. The Madeira Mode water which is seen in the model fields was not present in the initial conditions but was formed by the model during the course of integration. The width of the CWB has been reduced from over 500 km in the climatology to 200 km in the model. This is in better agreement with estimates based on hydrographic data.

3.5. T-S Curves

Selected T-S profiles from the averaged model fields are shown in Figure 5. The locations of the profiles are indicated in Figure 1a for profiles A-D. The bold lines in Figure 5 indicate the regimes of NACW and SACW as defined by *Tomczak* [1981]. Also indicated in the figure are MW, AAIW, and NADW for reference.
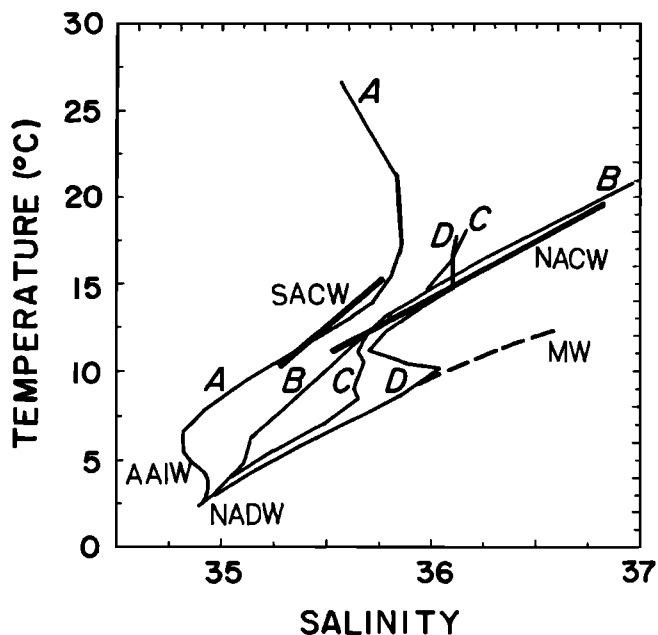
Fig. 5. T-S profiles; locations indicated in Figure 1a.

Profile A is located at 10°N, 20°W. SACW is clearly present between 10°C and 15°C. Below the SACW is AAIW between 8°C and 5°C. The coldest water is the NADW. The presence of SACW over AAIW and NADW was discussed in the previous section. Profile B (25°N, 35°W) is composed almost completely of NACW and NADW. In profile C (37°N, 15°W) the mixing of MW with NACW is seen between 6°C and 10°C. Overlying this MW is NACW, this is consistent with the northern end of the meridional section discussed earlier. The final profile is located very close to the Mediterranean outflow at 37°N, 10°W. Undiluted MW is found between 5°C and 10°C and NACW exists at temperatures warmer than 10°C.

4. EDDY VARIABILITY

Aspects of the three-dimensional structure of the eddy kinetic energy are described in section 4.1. The role of the mesoscale variability in the instability processes is presented in section 4.2. In section 4.3, these results are related to the model discretization and parameterizations.

4.1. Eddy Kinetic Energy

The eddy kinetic energy (K_E) at 1125 m is shown in Figure 6a. This depth has been chosen because of the availability of data and relevance to the formation of the Mediterranean salt tongue. The pattern at 1125 m is representative of the eddy variability in the upper thermocline, although the magnitudes are smaller at this depth. The K_E is largest between 15°N and 33°N and east to 20°W to 25°W. This is the region bounded to the north by the Azores Current and to the east and south by the Central Water Boundary. There are two other locations of significant K_E, one concentrated right along the coast of Africa and the other to the east of the Azores Islands (at 38°N, 15°W to 25°W). In the vicinity of the AC, K_E is generally 2-3 cm^2/s^2 with values as high as 4 cm^2/s^2. K_E is largest where the AC turns to the south and in the westward flowing recirculation region. Also indicated on the figure are the locations of moorings 831 (circle) and K276 (triangle). The measured kinetic energies are 5.9 cm^2/s^2 and 9.7 cm^2/s^2 for 831 and K276, respectively. The actual location of the moorings places them just to the north of the AC in the model fields. When compared to the historical position of the AC, they are located in the eastern part of the AC just as it begins to turn to the south, see Figure 1b. The analogous location in the model would be near 28°N, 29°W, where the model K_E are 2-3 cm^2/s^2, low by a factor of 2-5.

It is also of interest to study the vertical distribution of K_E in the Azores Current. The K_E as a function of depth is shown in Figure 6b for the model and three sets of current meter moorings. The model profile has been chosen to be
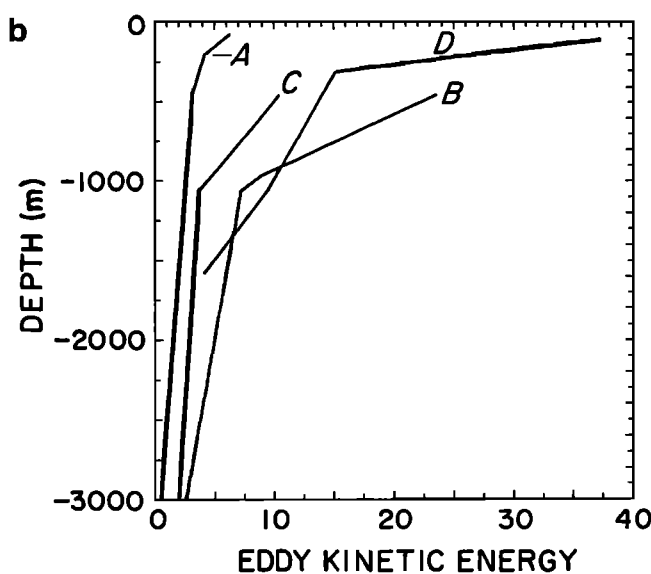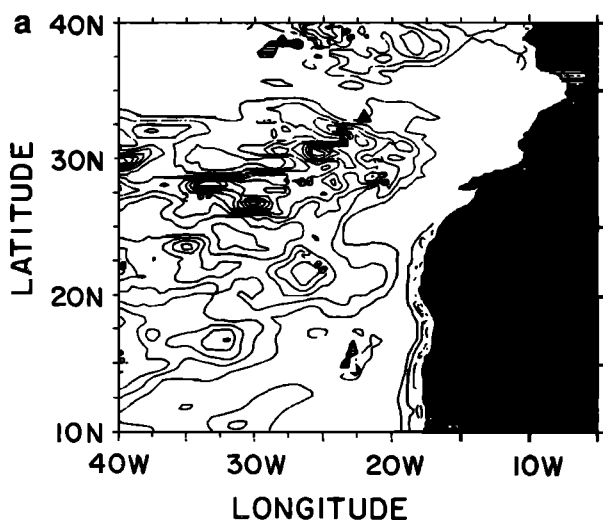
Fig. 6. Eddy kinetic energy (contour interval 0.5 cm^2 s^{-2}) : (a) eddy kinetic energy at 1125 m and (b) vertical profiles in the Azores Current for model and observations (A, model; B 831 first year; C 831 second year, D K276).

representative of the model K_E in the eastern extent of the AC and the moorings are K276 and 831, where mooring 831 has been broken up into its first and second years. The model K_E is significantly lower than that measured by the current meters, and the curvature of the model K_E is much too low in the upper ocean. Above 500 m the model K_E is between a factor of 3 and 6 lower than the measurements. At 1000 m, the model values are a factor of 2–5 less than the observations, and the deep values are low by a factor of 5.

It is evident from these figures that the K_E in the model AC is much lower than that measured by moored instruments. The upper thermocline distribution of K_E is similar to the map shown for 1125 m; the largest values are found near the Azores Current and Central Water Boundary, but they are still much less than estimates from observations. The low K_E reflected in the vertical profiles near the AC is found throughout the Canary Basin. Because the variability of the model fields is much less than the observed values, a detailed analysis of the kinetic energy budget would have questionable relevance to the real ocean and will not be done here. Instead, the analysis in the remainder of this section will concentrate on determining the reasons for this low K_E.

4.2. Energy Conversion by the Mesoscale Variability

The baroclinic and barotropic energy conversion between the mean and variable fields are calculated in the upper ocean. Comparisons are made with the limited estimates available from observations in terms of the magnitude, direction, location, and form of the energy conversion. While it has been stated that a detailed analysis of the eddy kinetic energy budget will not be done, the conversion terms are of interest because direct comparisons with previous observational and modeling analysis are possible. If the conversion rates are lower than these other estimates, this may be at least partially responsible for the low K_E found in the model fields.

One potential source of energy for the time variable fields is the potential energy of the time mean fields. This energy conversion is accomplished by the down density gradient flux of the perturbation density by the perturbation velocity field. This density flux has contributions due to both the temperature and salinity fields. In the following analysis, the discussion is presented in terms of the temperature flux only. The contributions due to the flux of salinity have been calculated and are in general agreement with the conclusions drawn from the temperature analysis.

The poleward eddy temperature flux has been calculated for the upper 500 m. The value of $\overline{v'T'}$ averaged over the upper 500 m and between 40°W and 25°W is shown as a function of latitude in Figure 7a. The largest fluxes are to the north along the AC (30°N) and to the south along the CWB. In the vicinity of the AC, the average value is approximately 0.0018°C cm s^{-1}. Also indicated in the figure are estimates of the eddy heat flux based on measurements across the AC by *Käse et al.* [1985], (hereinafter referred to as KZSH). Their measurements show a similar average value (0.002°C cm s^{-1}) with somewhat larger variability. The variability is not surprising since the model fluxes represent an average over two years of integration. The numerical modeling study by *Kielmann and Käse* [1987] of an idealized thin jet representation of the AC produced a similar north-

ward flux of 0.001°C cm s^{-1}. The positive temperature flux is an indication that the mean potential energy field is a source of energy for the fluctuations because the isotherms of the recirculation gyre shallow to the north in this region. The eddy temperature flux is to the south across the Central Water Boundary, between 14°N and 23°N, but there are no estimates available from observations.

The total conversion of mean potential energy to eddy energy is written in terms of the temperature as

$$S_{PE} = -\frac{\rho_0 g \alpha \overline{v'T'} T_y}{T_z} - \frac{\rho_0 g \alpha \overline{u'T'} T_x}{T_z} \qquad (1)$$

where contributions due to both the zonal and meridional mean temperature gradients are included. In (1), ρ_0 is the mean density of seawater, g is the gravitational acceleration, α is the coefficient of thermal expansion, T is the mean temperature field, and T' and u', v' are the eddy temperature and velocity components, respectively.

The baroclinic conversion rate averaged in the zonal and vertical directions is shown in Figure 7b as a function of latitude. The contribution due to meridional eddy fluxes is labeled as curve A, the zonal contribution is curve B, and the total is curve C. Negative values indicate that the net transfer of energy is from the mean to the eddy field. The Canary Basin falls into three-regions: 26°N to 36°N is the AC and its associated recirculation; 23°N to 26°N is the quiet water within the subtropical gyre; and 14°N to 23°N is the westward flow of the Central Water Boundary.

In the vicinity of the AC there are two distinct peaks in S_{PE}. The first is located at 30°N and is primarily due to the meridional component. This is associated with perturbations of the eastward flowing AC and the north-south gradient of the mean temperature field. The second peak is located at 33°N and is due to the zonal component. Analysis of the three dimensional fields indicates that this conversion source is located in the deep (300–500 m) western region at this latitude. The source of the potential energy is the zonal variation of the mean temperature field due to the reduction in size of the bowl shaped structure of the gyre recirculation with increasing depth.

The region south of the AC recirculation and north of the CWB is a region of low baroclinic instability. This is not surprising because it is within the recirculation gyre where the horizontal velocities and mean horizontal temperature gradients are small.

The temperature gradient along the CWB is another large source of eddy energy. The major contribution to the instability is due to the meridional component of the eddy heat flux. There are two peaks in energy conversions, located at 21°N and 17°N. These are the latitudes of the locally large K_E seen in Figure 6a along the CWB. This eddy variability is seen in the velocity field at 460 m on October 1 of the last year of model integration, shown in Figure 8. There are two wavelike patterns along the CWB at the latitudes of largest baroclinic conversion. These eddies are frequently seen along the CWB in the model, have baroclinic signatures from the surface to below 1500 m, and persist for time scales of 1 year. During this year, the wave packets propagate to the west along the CWB front where they interact and merge with the westward recirculation. Strong interleaving of the salinity front is often seen in hydrographic data off the coast of Africa near 20°W [*Zenk et al.*, 1989] and a similar pat-

(a) EDDY HEAT FLUX

(b) BAROCLINIC CONVERSION

(c) BAROTROPIC CONVERSION
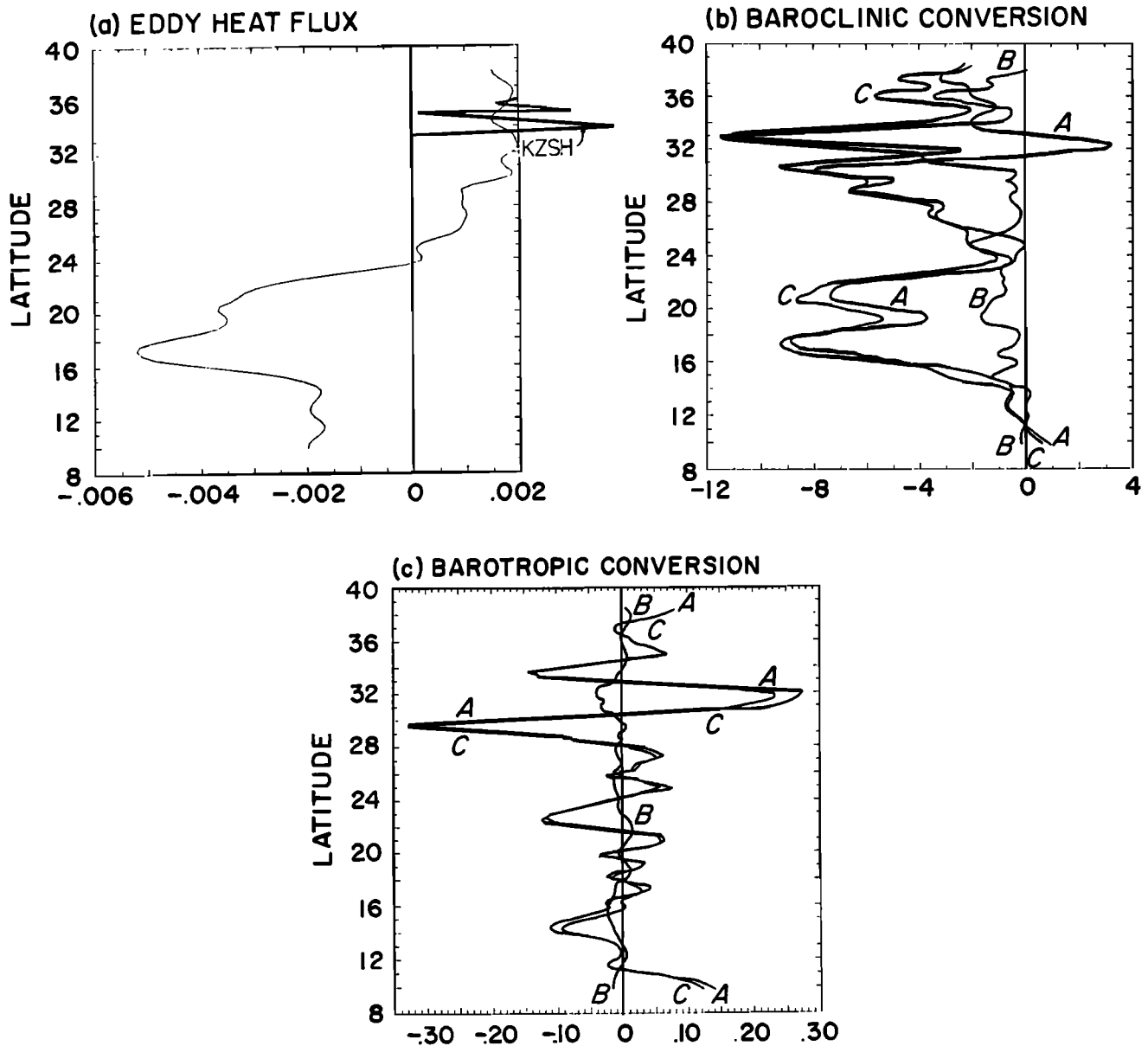
Fig. 7. Energy conversion by eddy variability: (a) meridional flux of temperature by eddy field ($^\circ$C cm s^{-1}), (b) baroclinic conversion of energy (10^{-6} J m^{-3} s^{-1}), and (c) barotropic conversion of energy (10^{-6} J m^{-3} s^{-1}).

tern has been observed in several float trajectories at 1000 m near this same location by Price et al. [1986] and Zemanovic et al. [1988]. Although it is not clear what a float trajectory in one of these model wave patterns might look like, the model fields do suggest that the variability found in the real floats and hydrographic data may be due to local baroclinic instability processes along the temperature gradient of the Central Water Boundary. If this is the case, the meandering of the CWB not only may be important to the local dynamics of the region, but may also act as a source of eddy variability to the western North Atlantic.

The largest value of the energy conversion rate in the AC is 1.1×10^{-5} J m^{-3} s^{-1}. The maximum found along the CWB is slightly lower, 0.9×10^{-5} J m^{-3} s^{-1}, but is active over a larger range of latitudes. These values compare with an estimate of 0.4×10^{-5} J m^{-3} s^{-1} from observations in the AC by KZSH. Part of the difference may be due to the fact

that KZSH did not consider the contribution from the zonal variation in the mean temperature gradient. It is important to note that, while the Azores Current is primarily zonal, it may interact with zonal variations of the large-scale density structure of the subtropical gyre circulation. Other conversion rates of 1.2×10^{-5} J m^{-3} s^{-1} have been calculated in the Antarctic Polar Front by Bryden [1979] and 1.5×10^{-4} J m^{-3} s^{-1} in the Iceland-Scotland Frontal Zone by Willebrand and Meincke [1980]. This indicates that baroclinic instabilities in the model are a significant source of eddy energy in the Canary Basin and are comparable to those rates found in similar fronts elsewhere in the ocean.

The mean kinetic energy field is also a potential source of energy for the eddy field. The total conversion from mean kinetic energy to eddy energy is written as

$$S_{KE} = \rho_0 \overline{u'v'} U_y + \rho_0 \overline{u'v'} U_x \qquad (2)$$
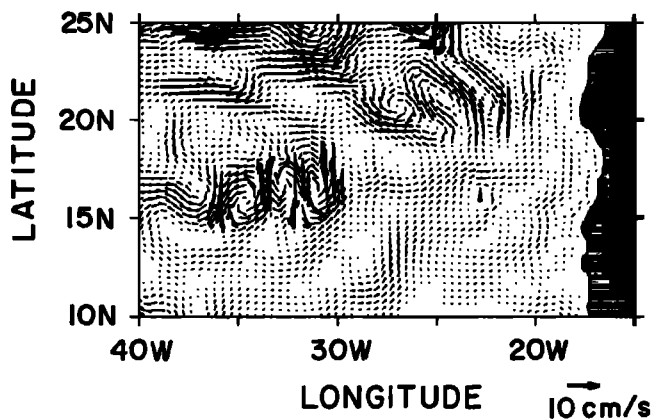
Fig. 8. Velocity at 460 m on October 1, model year 24.

The barotropic conversion rate averaged in the zonal and vertical directions is shown in Figure 7c as a function of latitude. In general, the magnitude of the barotropic conversion term is much smaller than the baroclinic term. At all latitudes, the meridional component is dominant over the zonal component. There are two distinct peaks, one over the southern portion of the AC and into the recirculation region (28°N to 30°N) and the other over the northern portion of the AC (30°N to 33°N). In the southern peak, the energy transfer is from mean kinetic energy to eddy energy. Between 30°N and 33°N the energy transfer is in the opposite direction; the eddy field is giving up its energy to the mean flow. Estimates of the barotropic conversion in the idealized numerical modeling study of Kielmann and Käse found a conversion from eddy to mean kinetic energy of 5.0×10^{-6} J m^{-3} s^{-1}, much larger than that found here. The lower conversion rate found in this study may be due to lower horizontal resolution (0.33° versus 0.1°) or the interaction of the Azores Current with the recirculation gyre. It is possible that the barotropic conversion in the AC is too small in this model but it is not believed that this is a major contributing factor to the low model K_E.

4.3. Model Parameterizations and Low K_E

In this section, several aspects of the model parameterizations which may influence the development and growth of eddies are discussed. It is impossible to say with any certainty if these numerical considerations are the cause of low K_E. The following analysis is intended only to point out likely areas which deserve further investigation. In the design of a numerical model for a given oceanic application there of course must be trade-offs. Many of the model parameters used in this first Community Modeling Effort were constrained by considerations other than the eddy kinetic energy structure. To name a few, computational requirements, suppression of gravity waves, and the progression from simple to more complex models all influenced the model design.

The horizontal resolution of the model is approximately 35 km and has been chosen to resolve geographical features such as the Florida Straits while remaining affordable in terms of computational requirements. In the Canary Basin, the Rossby radius of deformation varies from 60 km in the

south to 25 km in the north. Over much of the region the horizontal model resolution is the same or less than the radius of deformation. While the scale of most flow features is larger than this, energy exchange processes for geostrophic turbulence take place on scales of the Rossby radius. As such, adequately resolving this scale is likely to be important for an accurate representation of the flow of energy in the model. Although it is desirable to investigate the relationship between horizontal resolution and eddy energy, this is not yet computationally feasible on the scale of this numerical calculation. Possible alternatives include models with simplified geometry, nested and expandable grid models, and regional models.

The horizontal subgrid-scale parameterization is a biharmonic operator on the momentum and tracer variables. The biharmonic operator is more scale selective than the traditional Laplacian operator. The coefficient of horizontal diffusion used in the calculation was 2.5×10^{19} cm^4 s^{-1}, this is high for the horizontal resolution of the model and was required to maintain numerical stability. Analysis of a high resolution synoptic survey of the Azores Current and nearby recirculation by Käse et al. [1985] indicates that there are two dominant wavelengths, one at 570 km associated with the meandering of the AC and the other at 200 km associated with a mesoscale eddy field superimposed on the meandering jet Using the smaller of these two wavelengths, the estimated time scale of the horizontal friction term is 50 days. This is much shorter than time scales of dissipation generally believed to exist in the real ocean. Meddies, which are believed to be formed near the Mediterranean outflow, are only 100 km in diameter and have been tracked for up to 2 years, indicative of much weaker dissipation than the estimate for this model.

The coefficient of vertical viscosity in the momentum equations is 30 cm^2/s^2 and constant over the basin. This is 3–10 times larger than that which is typically used for primitive equation EGCM's. This large value was chosen to damp gravity wave generation which occurred on a very shallow shelf along the coast of Brazil, far from this region under study. The time scale of the vertical friction term in the upper thermocline is approximately 100 days. This is longer than, but comparable to, the horizontal friction term, and again it is much less than estimates for the real ocean. This rough scale analysis is consistent with the finding that, away from the NEC, the horizontal friction accounts for approximately 65% of the total K_E sink and the vertical friction accounts for the other 35%; bottom friction is very small. It is believed that reducing the horizontal and vertical dissipation used in this calculation will increase the eddy variability to be in better agreement with observational estimates.

The surface boundary condition on wind stress may influence the development of eddies in the ocean. The wind forcing has been filtered in both space and time. The time filtering eliminates all frequencies less than 2 months. The grid representation of the wind stress field has been subject to spatial smoothing through the analysis and mapping procedure of Hellerman and Rosenstein [1983]. In the real ocean, variability in the surface wind stress may directly force small-scale variability in the upper ocean, where it is subject to vertical diffusion and advection, into the ocean interior. The effect of high-frequency wind forcing on the generation of eddy variability in the ocean is an important question for the future development of numerical models and should be studied.

The surface boundary conditions on temperature and salinity may also influence the development of eddies. The salt flux at the surface is parameterized through a Newtonian damping term which relaxes the surface layer salinity back toward climatology. The climatological salinity field is smoothed in both space and time and will tend to suppress the mesoscale activity at the surface. The strength of this damping will be proportional to the time scale of the Newtonian term. A similar argument applies to the temperature field, although it is more complicated because the relaxation is calculated by a variable heat flux at the surface rather than a constant damping coefficient. The damping time scale for the salinity field is 50 days; this is also typical of the time constant derived through the heat flux relation for the temperature field.

The time rate of change of the eddy available potential energy (A') may be written in terms of the time rate of change of the perturbation temperature field as

$$A'_t = \frac{g\alpha T' T'_t}{2\overline{T_z}} \qquad (3)$$

$$T'_t = \frac{\gamma(T - T_R)}{C_p \rho \Delta Z} \qquad (4)$$

where $\alpha = 10^{-4} C^{-1}$, $\overline{T_z}$ is the vertical derivative of the temperature field, T_R is the reference value of the temperature for the surface heat flux, T' is the deviation of the surface temperature from T_R, C_p is the specific heat, ρ is the density of seawater, and ΔZ is the depth of the surface layer of water. The values chosen for the parameters were $\gamma/C_p\rho\Delta Z = 1/50$ days, $T' = 1°C$, and $\overline{T_z} = 0.03°C\ m^{-1}$. Using these values, the loss of eddy available potential energy through the surface boundary condition is 4.0×10^{-5} J $m^{-36}\ s^{-1}$ acting over the upper 50 m of water. This is compared to the generation of eddy energy by the conversion of mean available potential energy of 1.0×10^{-5} J $m^{-3}\ s^{-1}$ acting over the upper 500 m. This indicates that the loss of eddy energy through the upper boundary condition may be a significant portion of the generation in the upper 500 m by internal instability mechanisms. It is not known if this is a realistic representation of the actual ocean energy exchange process but indicates that further study in this area is needed.

5. OCEAN PROCESSES

In this section, the role of the current structure described in section 3 will be studied for three fundamental oceanic processes. In subsections 5.1, 5.2, and 5.3 the ventilation of the thermocline, meridional temperature flux, and formation of the Mediterranean salt tongue will be discussed.

5.1. Ventilation of the Thermocline

The ventilation of the thermocline is an important oceanic process. Accurate knowledge of the interaction of subsurface water with the atmosphere is important for ocean-atmosphere exchange of heat and CO_2. Ventilation of the ocean is also intricately tied to the general circulation through the conservation of potential vorticity [Luyten et al., 1983; Pedlosky et al., 1984]. Direct observations of thermocline ventilation are difficult to measure because it is believed to occur intermittently in space and time. The tradi-

tional approach has been to estimate the time since a parcel of water has interacted with the surface through the behavior of passive tracers such as oxygen and tritium. Several studies based on such data have indicated the presence of unventilated water in the eastern North Atlantic [Jenkins, 1987; Sarmiento, 1983]. This is in general agreement with the ventilated thermocline theory of Luyten et al. [1983], (hereinafter referred to as LPS83). In this section, the magnitude and mechanisms of ventilation in the Canary Basin will be calculated and compared with estimates based on observed tracer distributions.

The means by which ventilation is estimated in the numerical model is through a passive age tracer τ. The age of a water parcel is the time since that parcel has been in contact with the surface of the ocean. The age tracer equation is exactly like that of the active tracers except that an additional term is added which accumulates time (see Appendix A). The behavior of this passive tracer is quite similar to that of the age derived from the known behavior of tritium used by Jenkins [1987], hereinafter referred to as J87. At 15 years of integration the age tracer was started in the model calculation, hence the oldest value of τ in the model will be 10 years at the end of the 25 year integration. At each time step, the value of the tracer at the surface is set to zero.

The age at 91 m is shown in Figure 9a. There is a clear separation between the ventilated water to the north and the unventilated water to the south. This southeastern region is the shadow zone described by LPS83. Conservation of potential vorticity requires that water parcels, once subducted, leave the coast and are no longer in direct contact with the wind forcing. There is some evidence of an influence of the Equatorial Current near 10°N but this figure is in general agreement with basic ventilated thermocline theory.

The age field at 370 m gives a much different picture (Figure 9b). The front extending from the coast of Africa at 25°N is the shadow zone predicted by LPS83. As would be expected, the shadow zone has shifted to the north deeper in the water column. In the northwest corner of the domain the water is ventilated due to strong interaction with the winter mixed layer. Between these two regions, there are three subregions which differ from the smooth gradient which would be expected from Sverdrup flow. There is a tongue of ventilated water extending into the area from the west along 30°N, this is due to the AC. There is a second region which is nearly homogeneous further north and to the east, near 38°N. This is in the region of the meandering PC discussed in section 3. Finally, along the coast, there is ventilated water near the coast of Portugal. This is consistent with the southward extension of the winter mixed layer near the coast [Levitus, 1982].

An analysis of tritium fields was done in the Beta Triangle region centered at 27°N, 32.5°W (indicated in the figure) by J87. He found a general increase in age from the north to the south as is found here. The age varied from 3.5 at the northern apex of the triangle to 7.5 at the southern edge on the density surface $\sigma = 26.85$ (approximately 390 m). Those estimates compare quite well with those found in the model calculation. The age was also found to increase from 10 years at 20°N to 30 years at 10°N at 370 m along 38°W. This is in general agreement with the shadow zone found in the model fields but quantitative comparison is not possible because the model age is limited to 10 years.

From Figure 9b, it appears that the ventilation of the main thermocline is achieved by a mixture of direct Ekman
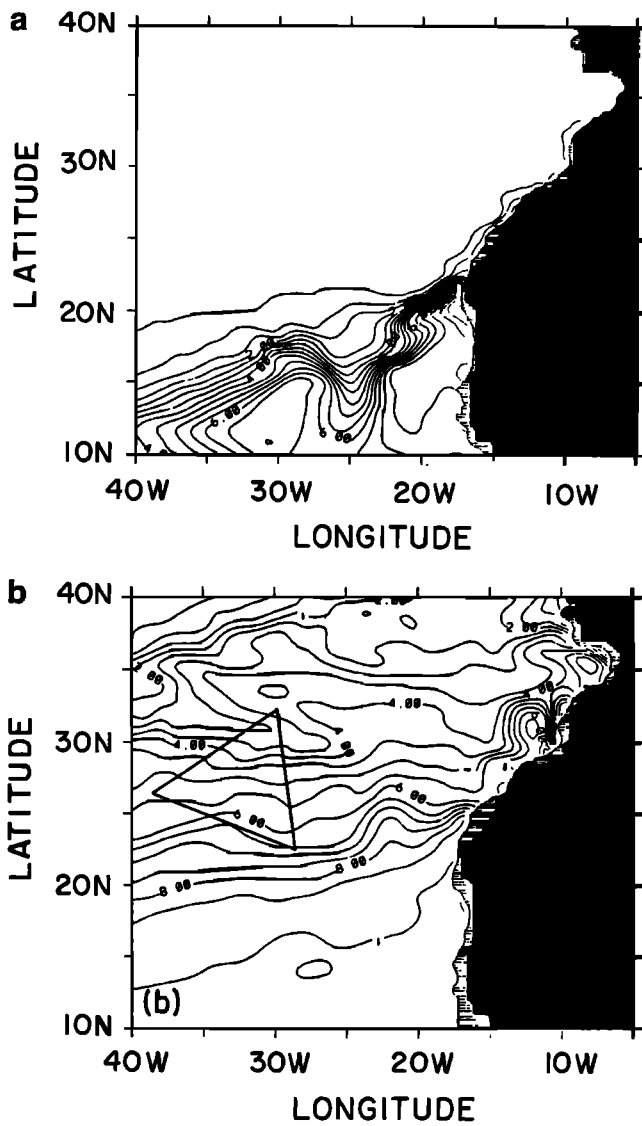
Fig. 9. Age tracer at (a) 91 m and (b) 370 m; contour interval 0.5 years.

Fig. 10. Subduction velocity: (a) at 260 m (contour interval 25, contours scaled by 1.0×10^{-8} m s^{-1} and (b) vertical profile (1.0×10^{-6} m s^{-1}; A, model in Beta Triangle; B, model in Azores Current; C, model in Portugal Current: D, J87 in Beta Triangle; and E, Ekman pumping.

pumping and horizontal advection of water renewed by wintertime convection. This is consistent with the results of J87 as he concluded that the recirculation is effectively ventilated "probably by passage through areas of deep winter convection." Although J87 considered convection regions only to the north, it appears here that the winter convection in the western North Atlantic is also a significant source of new water via the eastward flowing AC. A subduction velocity may be estimated as $W_s = f_0/f_T \tau_z$, where f_0 is the Coriolis parameter at the latitude of outcrop, f_T is the Coriolis parameter at the location of analysis, and τ_z is the vertical derivative of the age tracer (J87). This gives an estimate of the total subduction due to both the direct Ekman forcing and shoaling of the mixed layer. A less accurate estimate which makes no correction for conservation of potential vorticity is written as $W_s = \tau_z^{-1}$. Both measures will be used to study the relative contributions to thermocline ventilation.

The nonpotential vorticity conserving subduction velocity is shown in Figure 10a at a depth of 260 m. The contouring

has been limited to 5.0×10^{-6} m s^{-1} for presentation. The region south of the shadow zone is not valid for this analysis since all water in this region is essentially unventilated over the time of model integration. The subduction velocity is very large in the northwest because it is strongly influenced by wintertime convection. The effects of winter convection are also visible along the coast of Portugal. It is the area between the northern and south fronts that is of interest. The value of W_s is 1.26×10^{-6} m s^{-1} over most of the region, however, there are two large deviations from this base value. The first place is along the AC, where values are as large as 3.0×10^{-6} m s^{-1}. The second is in the region of the meandering PC, along 36°N, where values are also as large as

3.0×10^{-6} m s^{-1}. These compare with an Ekman subduction rate of approximately 0.85×10^{-6} s^{-1} for the outcropping of the $\sigma = 26.62$ density surface, or at approximately 258 m. At this depth, the Ekman pumping accounts for 67% of the total subduction over most of the region but in the areas of large mesoscale currents the shoaling of the mixed layer is dominant.

J87 calculated $\tau_z^{-1} = 1.25 \times 10^{-6}$ m s^{-1} at the center of the Beta Triangle at approximately 225 m. Although he did not look into the vertical derivatives over the rest of the triangle, there is evidence in his data of increased subduction at the northernmost apex of the Beta Triangle. The value of τ_z^{-1} calculated at 32.5°N, 30°W from the data of J87 indicates a subduction velocity of approximately 3.25×10^{-6} m s^{-1} at 225 m. These values compare quite well with the estimates from the age tracer in the model, both in the center of the Beta Triangle and at the northern apex. Based on the model analysis, the increased subduction to the north in the data of J87 may be evidence of ventilation by the Azores Current.

The vertical profile of the potential vorticity conserving subduction velocity is shown in Figure 10b for three locations in the model (curves A, B, and C), estimates from J87 (curve D), and Ekman pumping alone (curve E). Curve A is placed at the center of the Beta Triangle, at the same location as the estimates of J87, curve B is in the AC, and curve C is in the region of zonal jets of the PC.

Near the surface in the Beta Triangle, the Ekman pumping is a significant portion of the total subduction rate in both the model and J87 profiles. The contribution due to the Ekman pumping decreases with increasing depth. This is consistent with the reduction of Ekman pumping as one moves further north. The subduction velocity in the model Beta Triangle increases with increasing depth such that it is over 3.0×10^{-6} m s^{-1} at 500 m. This trend is consistent with the increase in the depth and horizontal gradient of the mixed layer as one moves north. The estimates by J87 also show a tendency to increase with depth so that it gives the same subduction rate as the model at 500 m. The subduction profile in the AC (curve B) is much different from that in the Beta Triangle. The near-surface subduction velocity is mostly due to shoaling of the mixed layer from the west, although the Ekman pumping is not negligible. The relative contribution due to shoaling remains almost constant with increasing depth; however, the overall ventilation decreases due to the reduction in Ekman pumping. The AC ventilation is much larger than that in the Beta Triangle in the upper 300 m. The AC ventilation does not increase with depth because the mixed layer does not go as deep in the western North Atlantic as it does to the north of this region. Curve C, in the PC, has the largest ventilation over the upper 500 m. Near the surface it is comparable to that in the AC, and at 500 m it is comparable to that in the Beta Triangle. Although always due to shoaling of the mixed layer, the upper ventilation is large because of the strong horizontal velocity field, and the deeper ventilation is large because of the steepening of the mixed layer depth further to the north.

5.2. Meridional Temperature Flux

The importance of the poleward heat transport by the atmosphere and oceans is well known. The purpose of analyzing the heat flux in the model fields is to determine

its magnitude, meridional and vertical distributions, source, and degree of ageostrophy.

The model fields are used to calculate the meridional temperature flux as a function of latitude and depth using the direct method. The sections taken in this subregion of the basin have a net mass transport; as such, the flux is referred to as a temperature flux instead of a heat flux. Zonal and vertical integrals will be taken in order to distill the large amount of information contained in the three-dimensional fields into a manageable result. The extent of the zonal integration is from 35°W to the coast, chosen to match the region of integration used in previous analysis of the historical data base by Stramma and Isemer [1986], (hereinafter referred to as SI). The vertical integration is done over the upper 1000 m, again to match the previous analysis and to contain the major components of the meridional temperature flux.

The three-dimensional velocity and temperature fields from the time-averaged model fields are used to calculate the meridional temperature flux, H, using the direct relation

$$H = \int \int \rho C_p \theta v \, dz \, dx \qquad (5)$$

where the integration is taken over depth and longitude, ρ is the density of seawater, C_p is the specific heat capacity of seawater (taken to be constant here), θ is the potential temperature, and v is the meridional component of velocity. The eddy component of the temperature flux has been calculated (section 4.2) and found to be negligible when compared to the mean flux.

The meridional temperature flux is shown in Figure 11a as a function of latitude for several flow representations. Negative fluxes are to the south. The curve marked A is the meridional flux of temperature using the full primitive equation velocity field from the model calculation. Curve B is the flux calculated using the geostrophic velocity derived from the model density field, relative to the primitive equation velocity at 1500 m. Curve C is the difference between curves A and B. Shown in Figure 11b are the temperature fluxes for the same region calculated by SI. In their calculations, they used a geostrophic velocity based on historical hydrographic data and an Ekman transport calculated from the average wind stress field. Triangles denote the total transport, geostrophic plus Ekman, and circles and crosses are the geostrophic and Ekman components, respectively.
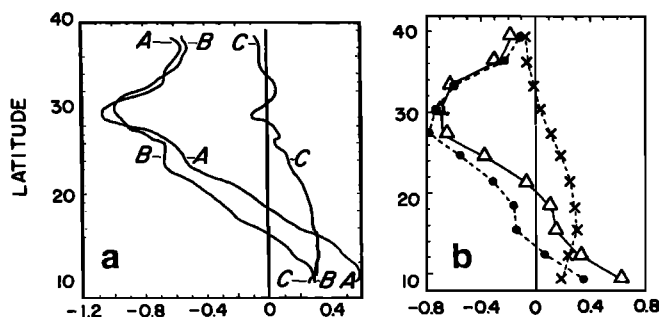
Fig. 11. Meridional temperature flux (times 10^{15}W), 0–1000 m: (a) from model (A, total; B, geostrophic; and C, ageostrophic) and (b) estimates from Strammer and Isemer [1986] (triangles total; circles, geostrophic; and crosses, Ekman).

In general, there is reasonable agreement between the model fluxes and those calculated by SI. At 38°N the total model flux (curve A) and the total flux estimated from observations (triangles) are to the south. The model flux is considerably larger, −0.65 PW compared to −0.23 PW, due to the larger transport in the Portugal Current produced by the model than was calculated by S84. The southward flux increases between 34°N and 30°N as the Azores Current enters the region from the west and turns to the south. The model produces a large southward flux of almost 1.1 PW compared to 0.7 PW from SI. The peak produced by the model at 29°N is due to the rapid southward turning of the AC discussed in section 3. Because the recirculation field calculated from the historical observations is much broader, the maximum in southward temperature flux does not show up as a narrow peak but is distributed over a larger range of latitude. Between 26°N and 10°N the model and SI show good agreement. The temperature flux continues to drop off rapidly as the southward flowing Portugal Current turns to the west and the NEC begins to transport temperature to the north. The reversal of the temperature flux occurs between 18°N and 19°N in the model and at 20°N in SI. At 10°N the northward flux is a maximum at 0.6 PW in both the model and SI.

It is also interesting to look at the differences between the primitive equation and geostrophic temperature flux from the model and compare them to the Ekman transport calculated from the surface wind stress. The ageostrophic component of the model flux is due to both the Ekman transport in the upper ocean and other ageostrophic contributions below the Ekman layer. The ageostrophic flux in the model follows very closely the flux due to the Ekman transport, curves C and X. North of 32°N the Ekman flux is to the south and is much smaller than the subsurface contribution. The similarity of the Ekman flux and the ageostrophic component of the model transport indicates that the primary ageostrophic contribution in the model is probably due to the Ekman transport.

Estimates of the poleward temperature flux in the North Atlantic have been made by *Hall and Bryden* [1982] with the direct method and IGY data at 24°30'N. Between the Bahamas and Africa they found a geostrophic southward transport of 1.58 PW. At the same latitude east of 35°W, the model produces 0.65 PW to the south, or approximately 40% of the estimated total southward transport. They calculated a northward heat flux due to Ekman transport of 0.53 PW compared to 0.15 PW in the model east of 35°W.

Currents responsible for the the integrated temperature fluxes just discussed will be further explored by looking at the distribution in the vertical. The depth dependence of the meridional temperature flux is shown in Figures 12a, b, and c for the primitive equation, geostrophic, and difference fields. These figures indicate that the field is meridionally inhomogeneous and strongly baroclinic. In Figure 12a there are two distinct regimes in the vertical. In the upper 35 m there is a layer of very strong temperature flux due to the Ekman transport. The Portugal Current (at 40°N) transports temperature to the south with local maxima at 75 m and 400 m. Below 800 m the flux due to the Portugal Current is very small. The southward turning of the Azores Current is clearly visible as two maxima in southward flux at 29°N, one at the surface and one at 350 m. Below 350 m, the temperature flux due to the AC is strongly baroclinic.

An interesting feature is the northward temperature flux at 32°N between 700 m and 1000 m. This is due to a branch of the Azores Current which splits and recirculates to the north near the base of the thermocline. South of the Azores, the flux becomes surface intensified as the Azores and Portugal Current recirculations turn to the west. The influx of SACW by the northward flowing NEC is seen down to 350 m between 10°N and 15°N.

The geostrophic temperature flux is shown in Figure 12b. The temperature flux due to the Ekman layer is not present in the geostrophic fields; the transport by the upper thermocline fields continues to increase up to the surface with the region 22°N to 32°N being strongly surface intensified. Below the near-surface layer the geostrophic fluxes are quite similar to the primitive equation fluxes. The difference fields are shown in Figure 12c. As discussed earlier, over most of the region the largest difference is due to the missing Ekman transport in the geostrophic fields. The upper 35 m shows a positive flux south of 33°N and a negative flux north of this latitude. There are only slight differences below the Ekman layer due to the upper thermocline flow field. In the AC and its recirculation the primitive equation fluxes are a few percent larger than the geostrophic fluxes.

5.3. Mediterranean Salt Tongue

In this section, the mechanisms of the formation of the Mediterranean salt tongue will be discussed. Specific questions to be addressed are: (1) how does the salt flux out of the Mediterranean region in the model compare to the observed flux; (2) how does this salinity anomaly get into the interior; (3) and why is the model salt tongue different from the observed salt tongue?

The Mediterranean basin is a region of net loss of water to the atmosphere through evaporation. As a result, there is a larger transport of water into the Mediterranean than returns to the North Atlantic. Because total salt must be conserved, the water which flows out of the Mediterranean through the Strait of Gibraltar is more saline than the surrounding North Atlantic water, giving rise to the Mediterranean salt tongue.

There is no explicit exchange of water between the North Atlantic and the Mediterranean Basin in the model because the horizontal resolution of the model is not sufficient to fully resolve the Strait of Gibraltar. The actual flow into the North Atlantic has been estimated to be approximately 1 Sv [*Bryden and Brady*, 1988]. This water mass interaction has been approximated through the addition of a Newtonian damping term to the tracer equations in the vicinity of the Gulf of Cadiz, as discussed in section 2.

The flux of salt relative to 35 ppt has been calculated through the boundaries of the control box shown in Figure 2b. Because of the damping term, flow leaving the region is generally of higher salinity than flow entering the region, giving rise to a net gain in salinity. Over the range of Mediterranean water in this region, 500 m to 1500 m, the net flux of salinity anomaly is 5.3×10^{12} kg/year. The anomalous flux of salt through the Strait of Gibraltar has been estimated by *Bryden and Brady* [1988] to be 50×10^{12} kg/year. The net salt flux in the model is only 10% of the estimated flux out of the Mediterranean. Although the Newtonian damping term does a good job of reproducing the observed temperature and salinity characteristics in the im-
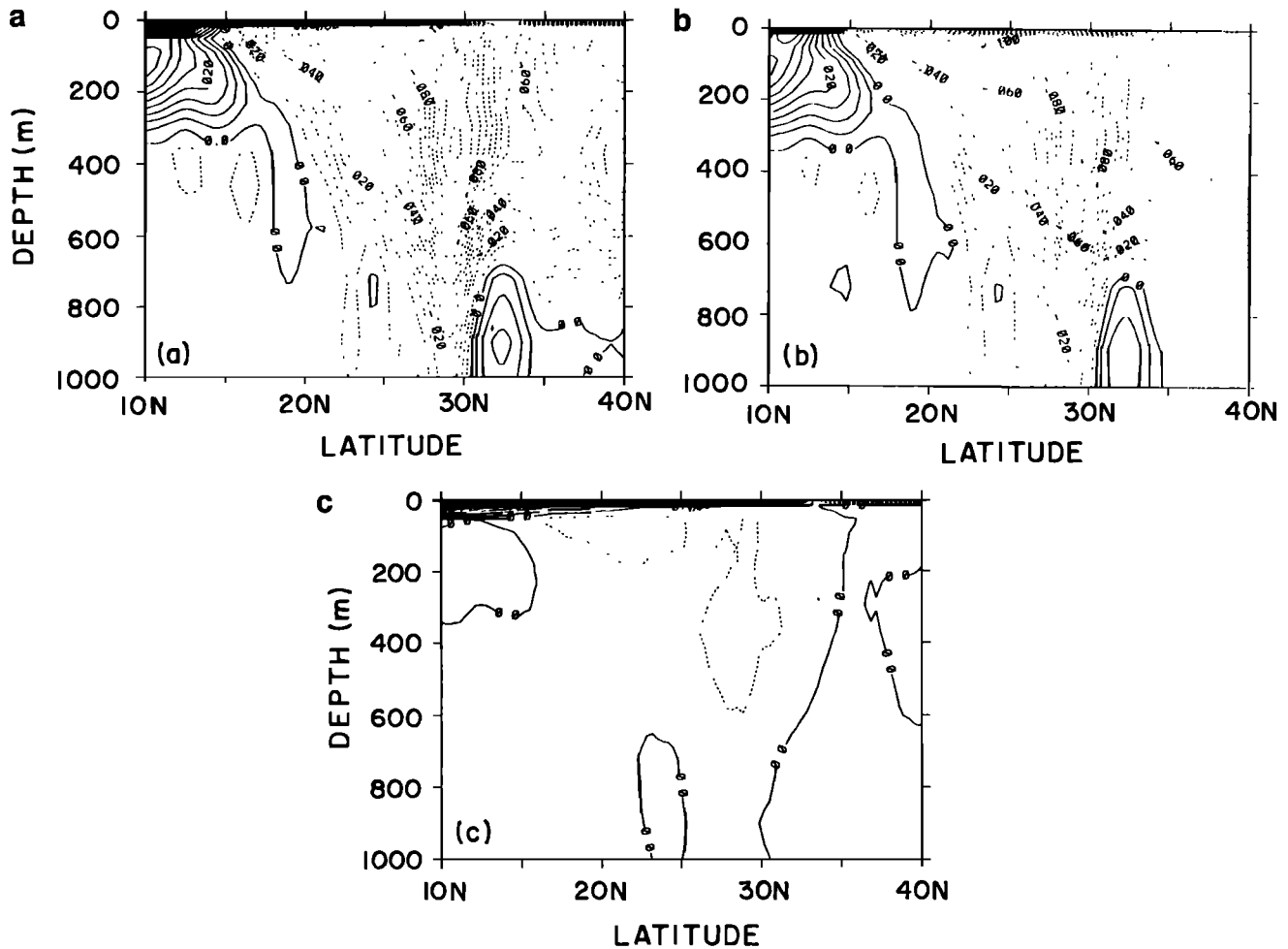
Fig. 12. Vertical profiles of temperature flux (contour interval 5×10^{-3} PW m^{-1}): (a) primitive equation flux (b) geostrophic flux, and (c) difference between primitive equation flux and geostrophic flux.

mediate vicinity of the outflow, it does not result in a sufficient flux of salinity. It is not believed that reducing the relaxation time would help significantly because the salinity within the damping region is already well represented. Another way to improve the salt flux might be to greatly increase the size of the damping region. This is not desirable because it would reduce the influence of the model dynamics and mesoscale variability, which are the main focus of this calculation.

There are two different concepts of the mechanism by which the large-scale, high-salinity water near the Mediterranean outflow gets into the interior of the North Atlantic. One theory is that the salinity acts as a passive tracer which is advected/diffused into the interior by the general circulation field. A second theory is that the Mediterranean water is not a passive tracer but has a density anomaly associated with it and as a result a geostrophic current which actively advects the Mediterranean water into the interior.

Shown in Figure 13 is the velocity superimposed on the salinity field at 1125 m in the vicinity of the salt tongue. The field is quite complex with mesoscale jets and eddies superimposed on the large-scale circulation. Along 20°W the core of the salt tongue protrudes into the more diluted water to the west in the form of long, mostly zonal, filaments (i.e.,

the 35.4 ppt contour). These features are quite long lived, at least 2 years. There is a strong correspondence between these salty filaments and the velocity field, with the high-salinity water generally to the right of the maximum velocity vectors. This circulation may be representative of realistic currents associated with the formation of the salt tongue or a result of the parameterization of the Mediterranean water outflow. If the climatology of the model ocean interior is different from the Levitus climatology to which the model fields are being forced in the vicinity of the Mediterranean outflow, a density gradient could result which would generate a geostrophic current between the damped and undamped regions. Because the mean model fields have not reached a steady state at this depth, it is not possible to determine if these currents are the result of such an imbalance.

The float data of Price et al. [1986] indicate the existence of a zonal jet of high-salinity water in the vicinity of 32°N, 25°W which persists for more than 1 year. Based on these data, they hypothesize that the Mediterranean salt tongue does not act as a passive tracer but is dynamically active and may have important internal dynamics. From their observations, it is not clear if the jet originates from the outflow at the Strait of Gibraltar or from mesoscale processes within the ocean interior. The model produces a similar structure
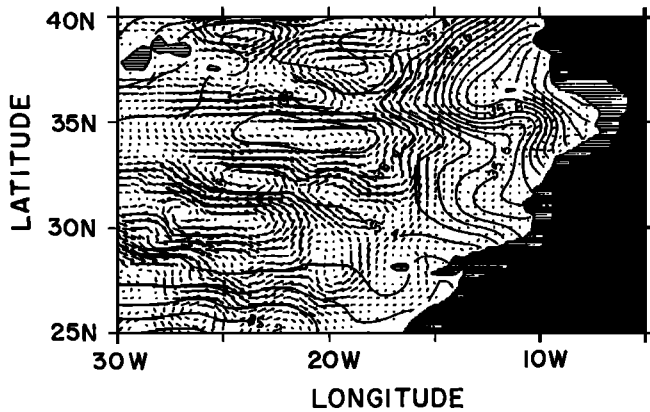
Fig. 13. Velocity and salinity at 1125 m; salinity contour interval 0.05 ppt.

without the explicit outflow from the Mediterranean. The source of the water for the model jet is the Azores Current, seen at this depth entering from the west at 30°N. The Azores Current does not have an anomalous salinity, but part of this flow interacts with the saltier water to the east before forming the westward jet. Although this similarity does not eliminate the possibility that the observed jet is due to some other process, it does indicate that such a feature can be formed from the mesoscale processes contained in this model.

Several processes related to the formation and maintenance of the Mediterranean salt tongue are not accurately represented in the numerical model. As was discussed earlier in this section, there is no explicit flow through the Strait of Gibraltar and the net flux of salt out of the region is much less than estimated from measurements. In addition, the horizontal resolution of the model grid is not sufficient to resolve the lenses of Mediterranean water (Meddies) which have been observed in the area [Armi et al., 1989; Richardson et al. 1989]. The Meddies are on the order of 100 km in diameter and 1000 m thick. Estimates of Richardson et al. [1989] place the transport of salinity anomaly due to Meddies at approximately 20% of the total flux into the North Atlantic through the Strait of Gibraltar. It is likely that these processes are important to the dynamical balance in the Mediterranean salt tongue, and as such, the analysis of the dynamical balance in the model salt tongue has been limited to the discussion of the zonal filaments as a possible mechanism for offshore transport of Mediterranean water.

6. CONCLUSIONS

The Canary Basin region of an eddy-resolving, general circulation model of the North Atlantic Basin has been studied in terms of its mean velocity and density structure, eddy variability, and its role in three fundamental oceanic processes. The model calculation was carried out by Bryan and Holland [1989] as the first Community Modeling Effort in the World Ocean Circulation Experiment. The three major currents flowing into the Canary Basin are the Azores Current, the Portugal Current, and the North Equatorial Current. The transports and locations of each of these currents in the mean model fields compare reasonably well with

estimates based on observations. The model dynamics have introduced fine horizontal and vertical scales to the initially coarse climatological representation of the temperature and salinity fields. Some aspects of the density fields were improved while others were degraded. The two major deficiencies of the model fields are the representation of the Mediterranean salt tongue and eddy kinetic energy values which are 2 to 6 times too low.

The Canary Basin has been shown to be important to the general circulation through the meridional flux of temperature, formation of the Mediterranean salt tongue, and ventilation of the thermocline. The temperature flux was found to have a meridional structure similar to that of the geostrophic advection of the climatological temperature field, although the model generally had larger equatorward transports. The dominant ageostrophic contribution was due to the Ekman transport in the upper 35 m. This indicates that estimates of subsurface temperature fluxes based on a geostrophic balance is probably sufficient. The Newtonian damping parameterization of the Mediterranean outflow was found to reproduce the water properties near the outflow quite well but produced only 10% of the estimated flux of salinity anomaly out of the region. It is believed that this low salt flux is at least partially responsible for the difference seen between the model salt tongue and climatology. Dynamically active zonal filaments of high-salinity water are proposed as a mechanism to transport salt from the coastal region into the interior. Ventilation of the thermocline was studied using a passive age tracer in the model. In the Beta Triangle area, the model age and ventilation rates compare quite well with estimates based on tritium observations. At 370 m there is a mix of ventilation due to the Ekman pumping of the basic ventilated thermocline theory and shoaling of distant mixed layers due to mesoscale jets and eddies. The Azores and Portugal currents were both found to be effective means of ventilation in the model. The implication is that ventilation is a complicated and inhomogeneous process involving direct and distant wind forcing and large and mesoscale circulations.

Based on this analysis, several recommendations can be made to the modeling community. A major deficiency of the model fields is the representation of the Mediterranean salt tongue. Alternatives to the parameterization of the Mediterranean outflow must be studied, including explicit water exchange, sensitivity to resolution, and form of the open boundary conditions. The second major discrepancy between the model and observations is the low value of eddy kinetic energy. The horizontal and vertical viscosity, horizontal resolution, and surface boundary conditions are suggested as topics for future study. A third shortcoming of the model calculation is the location and transport of the Azores Current. The dominant forcing mechanisms of the Azores Current are not known, so this result cannot yet be attributed to any aspect of the numerical model. The computational expense of the model precludes extensive physical/computational parameter studies on this scale. To further investigate the relation of the model numerics to the physical processes just discussed, simpler models, both numerical and analytical, must be used to isolate the dominant forcing mechanisms and function of the numerical parameterizations. These aspects of the calculation should be better understood before the next step in the evolution of this class model.

These results have described several mesoscale processes not previously found in the observations. If actually present in the ocean, many of these mesoscale features may play an important role in the fundamental processes studied in this paper. As such, and in order to test and improve future model developments, observational programs should consider these processes in the design and analysis of future experiments. Does a low-frequency, zonal wave pattern exist superimposed on the Portugal Current? Are dynamically active filaments of salt present in the salt tongue and, if so, are they an important mechanism of transport into the interior? Does a deep, anticyclonic circulation exist over the Canary Abyssal Plain? Is the Central Water Boundary a region of baroclinic instability? To what extent is the Canary Basin ventilated by mesoscale features such as the Azores Current?

APPENDIX A

The equations of motion solved in the numerical integration of Bryan and Holland [1989] are presented in this section. Only a brief summary will be given here; details of the calculation can be found in the reference.

It is first useful to define the advective operator $\Gamma(\mu)$ as

$$\Gamma(\mu) = ma^{-1}[(u\mu)_\lambda + (v\mu^{-1})_\theta] + (w\mu)_z \qquad (6)$$

Where $u = a\lambda_t/m$, $v = a\theta_t$, $m = \sec(\theta)$, θ is the latitude, λ is the longitude, and a is the radius of the Earth.

The λ, θ, and z momentum equations are written as

$$u_t + \Gamma(u) - fv = -ma^{-1}(P/\rho_0)_\lambda + F^u \qquad (7)$$

$$v_t + \Gamma(v) + fu = -a^{-1}(P/\rho_0)_\theta + F^v \qquad (8)$$

$$P_z - \rho g = 0 \qquad (9)$$

where $f = 2\Omega\sin(\theta)$, ρ_0 is the mean density (taken to be unity), and P is the pressure. F^u and F^v are parameterizations of subgrid-scale processes.

The conservation of mass for an incompressible fluid gives the continuity equation

$$\Gamma(1) = 0 \qquad (10)$$

Equations are written for the active tracers temperature (T) and salinity (S) and the passive age tracer (A) as

$$T_t + \Gamma(T) = F^T \qquad (11)$$

$$S_t + \Gamma(S) = F^T \qquad (12)$$

$$A_t + \Gamma(A) = F^T + 1 \qquad (13)$$

where F^T is the parameterization of subgrid-scale processes for each of the tracers. An equation of state is used to close the system.

$$\rho = \rho(T, S, P) \qquad (14)$$

In the present model, the equation of state is represented by a polynomial fit to the Knudsen formula [Bryan and Cox, 1972].

The subgrid-scale processes are parameterized with a second-order operator in the vertical and a biharmonic operator in the horizontal.

$$F^\mu = A_h \nabla^4(\mu) + A_v \mu_{zz} \qquad (15)$$

A_h is the horizontal diffusion coefficient ($2.5 \times 10^{19} \text{cm}^4 \text{ s}^{-1}$) and A_v is the vertical diffusion coefficient ($30\text{cm}^2 \text{ s}^{-1}$).

REFERENCES

Armi, L. and D. Haidvogel, Effects of variable and anisotropic diffusivities in a steady state diffusion model, *J. Phys. Oceanogr.*, *12*, 785–794, 1982.

Armi, L., and H. Stommel, Four views of a portion of the North Atlantic Subtropical Gyre, *J. Phys. Oceanogr.*, *13*, 828–857, 1982.

Armi, L., D. Herbert, N. Oakey, J. F. Price, P. L. Richardson, H. T. Rossby and B. Ruddick, Two years in the life of a Mediterranean salt lense, J. Phys. Oceanogr., 19, 354–370, 1989.

Bryan, F. O. and W. R. Holland, A high resolution simulation of the wind- and thermohaline-driven circulation of the North Atlantic Ocean, Paper presented at Hawaiian Winter Workshop: Parameterizations of small scale processes, Univ. of Hawaii, Jan 17-20, 1989. Sponsored by U. S. Office of Naval Research, Hawaiian Inst. of Geophysics, and Dept. of Oceanogr. Univ. of Hawaii.

Bryan, K. and M. D. Cox, A numerical investigation of the oceanic general circulation, *Tellus, 19*, 54–80, 1967.

Bryan, K. and M. D. Cox, An appropriate equation of state for numerical models of ocean circulation, *J. Phys. Oceanogr., 2*, 510–514, 1972.

Bryden, H. Poleward heat flux and conversion of available potential energy in the Drake Passage, *J. Mar. Res., 37*, 1–22, 1979.

Bryden, H. L. and E. C. Brady, R. D. Pillsbury, Flow through the Strait of Gibraltar, Paper presented at Gibraltar. *Seminario Sobre Oceanografia Fisica Del Estrecho De Gibraltar, Madric, Octubre, 24-28*, 1988, SECEG, Madric, 166–194.

Camp, N. T. and R. L. Elsberry, Oceanic thermal response to strong atmospheric forcing, II, The role of one dimensional process, *J. Phys. Oceanogr., 8*, 215–224, 1978.

Dickson, R. R. and W. J. Gould and T. J. Muller and C. Maillard, Estimates of the mean circulation in the deep (>2000m) layer of the eastern North Atlantic, *Prog. Oceanogr., 14*, 1985,

Dietrich, G. and K. Kalle and W. Krauss and G. Siedler, *General Oceanography*, John Wiley, New York, 626 pp, 1980.

Gould, W. J., Physical oceanography of the Azores front, *Prog. Oceanogr., 14*, 167–190, 1985.

Hall, M. M. and H. L. Bryden, Direct estimates and mechanisms of ocean heat transport, *Deep Sea Res. 29*, 339–359, 1982.

Han, Y. J., A numerical world ocean general circulation model. Part II, A baroclinic experiment, *Dyn. Atmos. Oceans. 8*, 141–172, 1984.

Hellerman, S. and M. Rosenstein, Normal monthly wind stress over the world ocean with error estimates, *J. Phys. Oceanogr., 13* 1093–1104, 1983.

Hellerman, S., Charts of the Variability of the wind stress over the Atlantic, *Deep Sea Res., 26*, 63–75, 1980.

Jenkins, W. J., H and He in the beta triangle: Observations of gyre ventilation and oxygen utilization rates, *J. Phys. Oceanogr., 17*, 763-783, 1987,

Käse, R. H. and J.F. Price and P.L. Richardson and W. Zenk, A quasi-synoptic survey of the thermocline circulation and water mass distribution within the canary basin, *J. Geophys. Res.*, *91*, 9739-9748, 1986.

Käse, R. H. and A. Beckmann and H. Hinrichsen, Observational evidence of salt lens formation in the Iberian Basin, journal, *J. Geophys. Res.*, *94*, 4905-4912, 1989.

Käse, R.H. and W. Zenk and T.B. Sanford and W. Hiller, Currents, Fronts, and eddy fluxes in the canary basin, journal, *Prog. Oceanogr.*, *14*, 231-257, 1985.

Kielmann, J. and R.H. Käse, Numerical modeling of meander and eddy formation in the Azores current frontal zone, *J. Phys. Oceanogr.* *17*,, 529-541, 1987.

Levitus, S., Climatological atlas of the world ocean, *NOAA Prof. Pap.*, *13*, 173pp., 1982.

Luyten, J. R., J. Pedlosky and H. Stommel, The ventilated thermocline, *J. Phys. Oceanogr.*, *13*, 292-309, 1983,

Maillard, C. and R. Käse, The near surface flow in the subtropical gyre south of the Azores, *J. Geophys. Res.*, *94*, 16133-16140, 1989.

Pedlosky, J., W. Smith and J. R. Luyten, On the dynamics of the coupled mixed layer-thermocline system and the determination of the oceanic surface density, *J. Phys. Oceanogr.*, *14*, 1159-1171, 1984,

Price, J. F., T. K. McKee, J. R. Valdes, P. L. Richardson, L. Armi, SOFAR float Mediterranean outflow experiment, 1984-1985, Tech. Rep., WHOI-86-31, 199pp., Woods Hole Oceanogr. Inst., Woods Hole, MA., 1986.

Richardson, P. L. and K. Mooney, The Mediterranean outflow - a simple advection-diffusion model, *J. Phys. Oceanogr.*, *5*, 476-482, 1975.

Richardson, P. L., D. Walsh, L. Armi, M. Schroder, J. F. Price, Tracking three Meddies with SOFAR floats, *J. Phys. Oceanogr.*, *19*, 371-383, 1989.

Sarmiento, J. L., A Tritium box model of the North Atlantic thermocline, *J. Phys. Ocean.*, *13*, 1269-1274, 1983.

Saunders, P. M., Circulation in the eastern North Atlantic, *J. Mar. Res.*, *40*, 641-657, 1982.

Schmitz, W. J. and J. F. Price, P. L. Richardson, Recent moored current meter and SOFAR float observations in the eastern Atlantic near 32°N, *J. Mar. Res.*, *46*, 301-319, 1988.

Siedler, G. and A. Kuhl, W. Zenk, The Madeira Mode water, *J. Phys. Ocean, 17*, 1561-1570, 1987.

Stramma, L. and H. Isemer, Seasonal variability of meridional temperature fluxes in the eastern North Atlantic, *J. Mar. Res.*, *46*, 281-299, 1988,

Stramma, L. and G. Siedler, Seasonal changes in the North Atlantic subtropical gyre, *J. Geophys. Res.*, *93*, 8111-8118, 1988.

Stramma, L. and H. Isemer, Meridional temperature fluxes in the subtropical eastern North Atlantic, *Deep Sea Res.*, *33*, 209-223, 1986.

Stramma, L., Geostrophic transport in the warm water sphere of the eastern subtropical North Atlantic, *J. Mar. Res. 42*, 537-558, 1984.

Sverdrup, H. U. and U. W. Johnson, R. H. Flemming, *The Oceans*, Prentice-Hall, Englewood Cliffs, N. J., 1087pp.,1942.

Tomczak, M., An analysis of mixing in the frontal zone of South and North Atlantic central water off Northwest Africa, *Prog. Oceanogr.*, *10*, 173-192, 1981.

Willebrand, J. and J. Meincke, Statistical analysis of fluxuations in the Iceland-Scotland frontal zone, *Deep Sea Res. 27*,, 1047-1066, 1980.

Zemanovic, M. E. and P. L. Richardson, J. R. Valdes, J. F. Price, L. Armi, SOFAR float Mediterranean outflow experiment data from the second year, 1985-1986", Tech. Rep., WHOI-88-43, 230pp., Woods Hole Oceanographic Inst., Woods Hole, MA, 1988.

Zenk, W. and B. Klein, M. Schroder, Cape Verde frontal zone, *Deep Sea Res., in press*, 1989.

Zenk, W and T. J. Muller, Seven year current meter record in the eastern North Atlantic, *Deep Sea Res.*, *35*, 1259-1268, 1988.

M. A. Spall, Woods Hole Oceanographic Institution, Woods Hole, MA 02543.